Research Article

For reprint orders, please contact: reprints@futuremedicine.com

Nanomedicine

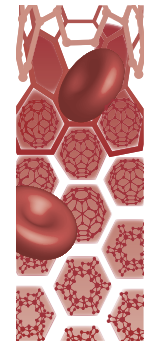

Mesoporous gold nanoparticles for photothermal controlled anticancer drug delivery

Lingling Zhang[1], Sida Shen[2], Liang Cheng**[,2], Hongjun You[3], Lu Lu[4], Chuansheng Ma[4], Yanzhu Dai[4] & Jixiang Fang*[,1]

[1]School of Electronic & Information Engineering, Xi'an Jiaotong University, Xi'an, Shann xi 710049, PR China

[2]Institute of Functional Nano & Soft Materials (FUNSOM), Collaborative Innovation Center of Suzhou Nano Science & Technology, Soochow University, Suzhou, Jiangsu 215123, PR China

[3]School of Science, Xi'an Jiaotong University, Xi'an, Shann xi 710049, PR China

[4]School of Microelectronics, Xi'an Jiaotong University, Xi'an, Shann xi 710049, PR China

*Author for correspondence: jxfang@mail.xjtu.edu.cn

**Author for correspondence: lcheng2@suda.edu.cn

Aim: To realize the transit and release of cancer drug exactly as well as high drug loading ratio, we reported a biocompatible and temperature responsive controlled drug delivery system based on 3D mesoporous structured Au networks. **Materials & methods:** Here, we filled the hollow interiors of Au networks with a phase-change material so that the drug release was easily regulated by controlling the temperature only. **Results:** Thanks to the high near-infrared reflectance absorbance and mesoporous structure, the Au–PEG + lauric acid/doxorubicin system showed a strong photothermal conversion efficiency, high drug-loading ratio (54.2% for doxorubicin) and controlled drug release. **Conclusion:** This system revealed great advantages in photothermal therapy and chemotherapy, offering an obvious synergistic effect in cancer treatment.

First draft submitted: 13 July 2018; Accepted for publication: 13 March 2019; Published online: 6 June 2019

Keywords: Au networks • cancer treatment • drug control release • high drug-loading ratio • phase-change material

Owing to the feature of uncontrolled cellular growth, cancer is becoming one of the leading causes of death all over the world. The primary approaches of cancer therapy contain surgery, radiation therapy and chemotherapy, which usually kill healthy cells and lead to cancer recurrence [1,2]. Recently, nanotechnology combined treatments with phototherapy, radiotherapy and chemotherapy, as a new method for the diagnosis, monitoring and cure of disease, has garnered much attention in the biomedical field due to its large specific surface, high surface activity and strong antioxidant property at the molecular level [3]. To reduce the toxicity of an anticancer drug and raise the circulation effect, different controlled drug delivery systems have been exploited, such as liposome [4,5], polymeric micelle [6], graphene [7,8], carbon-based nanomaterials [9], magnetic nanoparticles [10], mesoporous silica nanoparticles [11,12], metallic nanoparticles [13] and so on.

Among these materials, noble metals, especially Au nanomaterials, have been explored diffusely in the treatment of cancer: photothermal therapy (PTT), drug delivery and cancer cell imaging [14]. In PTT, thanks to their absorption in the near-infrared reflectance (NIR) from 700 to 900 nm, cancer cells are burnt by heat generated from optical energy through highly efficient photothermal agents. Meanwhile, loaded with drugs in different formulations, Au nanoparticles are able to release agents in pathological cellular without damaging normal cells [15]. Furthermore, the metal ions can be served as contrast agents for photoacoustic imaging, adding a unique capability to resolve and track *in vivo* location of a drug delivery system [16].

Nowadays, typical efforts have been made to synthesize high-quality and various-morphology Au nanomaterials for cancer therapy, for example nanoparticles, nanowires, nanosheets and nanocages [1]. What is more, several strategies of modifying the surface of Au nanomaterials have been investigated, including surface coating method and ligand exchange method, so that they can be better applied in cancer therapy [17–19]. However, to our best

Future Medicine

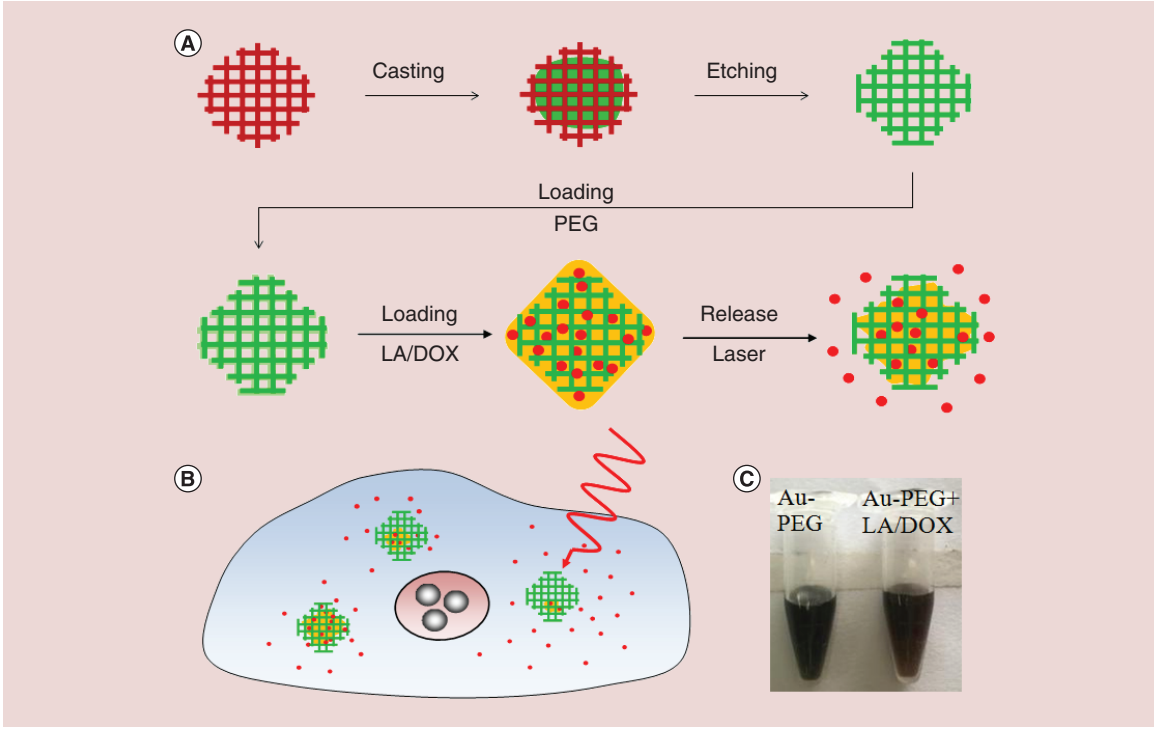

Figure 1. Photographs of synthesis Au networks and their biomedical application. (A) Schematic illustrating synthesis of Au networks in KIT-6 hard template, DOX loading into Au networks by LA then releasing by photothermal effect. The red networks represent the hard template and the green networks represent the resulting gold networks after removing the hard template. **(B)** Schematic illustrating drug release under the laser irradiation. **(C)** Photos of Au–PEG and Au–PEG + LA/DOX in water.
DOX: Doxorubicin; LA: Lauric acid; PEG: Polyethene glycol.

knowledge, there are no Au nanomaterials, apart from nanocages, that have been widely used for biological drug delivery. Although we could deliver cancer drug to a specific target and control it release by light [20], pH [21–23], electrochemistry [24] and phase change material [25,26], it is a not easy task to realize ideal control of drug release in a more convenient and simple way. What is more, very few studies have reported the doxorubicin (DOX) delivery with high-loading ratio. It is difficult for drugs to be attached at the surface or diffuse into the interior of a solid Au nanoparticle even with a more complex structure [27], which renders a lower drug loading ratio and a waste of the loading potential of delivery. Previous studies have provided plenty of strategies to assist drug delivery systems in loading anticarcinogen, including pH-sensitive linkers [23], phase change materials [25]. To date, a robust carrier delivering DOX has not been achieved more than 35% with a simple synthesis method [28]. Therefore, it is crucial to develop a carrier that is capable of delivering drugs and releasing them in a spatial as well as high drug loading.

Recently, the author has reported 3D mesoporous structured Au networks synthesized by means of a general soft-enveloping strategy in the template limited space [29] and pioneered the application of them to cancer therapy. In fact, owing to ultrahigh specific surface area, mesoporous and hollow interior, good biocompatibility as well as excellent photothermal performance, 3D mesoporous Au networks represented a new class of multifunctional drug delivery carrier for the combined photothermal-chemotherapy. Figure 1A showed a schematic diagram of the encapsulation of anticancer drug and release mechanism. We used a KIT-6 hard template (the red networks) to prepare mesoporous Au networks (the green networks) through a chemical reduction. Since the mesoporous structure, the Au networks have high drug loading up to 54.2%, much higher than the previously reported Au nanomaterials (usually below 35%). And we used lauric acid (LA) as the medium (Au–PEG + LA) to control the drug loading and release in response to temperature increase. Exposed to laser or direct heating, the LA molecule would melt and escape from the interior of Au networks through the small channel of Au networks, concurrently releasing the anticancer drug delivery into the surrounding, which provided a simple way to control the drug release (Figure 1B). Moreover, owing to the high absorption in NIR, the final system of Au–PEG + LA/DOX offered an

apparent photothermal. Therefore, this system reported here may provide a better insight to handle drugs deliver and synergistic effect for biological therapy.

Materials & methods

Chemicals

KIT-6 was purchased from Nanjing Material Tech. Co., Ltd. Chloroauric acid ($HAuCl_4.3H_2O$, ≥99.9%), ethanol (C_2H_5OH, ≥99.5%), hexane (C_6H_{14}, ≥99.5%), lipoic acid (LA, ≥99.0%0), methoxypolyethylene glycol amine (mPEG-NH_2, ≥99.5%), dichloromethane (CH_2Cl_2, ≥99.8%), N,N′-dicyclohexylarbodiimide (DCC, ≥99.0%), triethylamine (TEA, ≥99.5%), DOX (removing hydrochloride, DOX, ≥98.0%), LA (≥98.0%), methanol (CH_3OH, ≥99.9%), methyl thiazolyltetrazolium (MTT, ≥98.0%) were obtained from Sinopharm Chemical Industry Co., Ltd. 1,1,3,3-tetramethyldisiloxane (TMDS, ≥97.0%) and hydrofluoric acid (HF, ≥40.0%) were obtained from Shanghai Aladdin Biochemical Technology Co., Ltd. Murine breast cancer cells (4T1) were obtained from American Type Culture Collection.

Synthesis of 3D ordered mesoporous Au networks

In a typical impregnation process, the dried KIT-6 (0.1 g) powder was mixed with $HAuCl_4$ (3 mM, 10 ml) ethanol solution. After the complete drying under reduced vacuum condition, the powder was dispersed in 1 ml hexane. And then the 3D ordered mesoporous Au networks were obtained through the chemical reduction (TMDS, 100 µl), removing silica template (HF, 20%) and washing with distilled water and ethanol according to a protocol described in our previous report [29], referred to as Au networks.

Surface modification of Au networks with lauric acid

PEG polymer was synthesized following a previous protocol [30]. For PEG coating, 20 mg Au networks dispersed in 5 ml H_2O were mixed with 50 mg PEG. After ultrasonication for 30 min and stirring overnight, excess PEG molecules were removed by centrifugation at 14,800 rpm and repeated water washing. The final Au–PEG networks were resuspended in H_2O at the concentration of approximately 2 mg/ml for further use.

Loading Au networks doxorubicin

The obtained Au–PEG networks were centrifuged and redispersed in methanol. DOX (removing hydrochloride, DOX) and LA were first mixed in methanol and then added into the above Au–PEG methanol solution and heated at 50°C for 6 h, followed by increasing the temperature to 70°C to evaporate methanol. Then the above mixture was cooled down to room temperature and stirred for half an hour after dissolved with water. The final Au–PEG + LA/DOX networks were collected by centrifugation at 14,800 rpm and washed with methanol and water twice, respectively, and fixed volume to 1 ml, diluted 50-times. After equilibration, the drug solution was assayed by UV–visible spectrophotometry at a wavelength of 480 nm. The percentage of drug loading onto the resin was calculated by the following equation:

$$\%\ \text{Drug loading} = [(D_{IN} - D_{EQ}/W)] * 100 \quad (1)$$

Where, D_{IN} and D_{EQ} are the drug contents at the initial and after equilibration, respectively. W is the resin used content for drug loading.

The final product was dispersed in water and stored at 4°C for future use.

DOX release from the Au–PEG by heating

To study the release of DOX, Au–PEG + LA/DOX solution in pH 7.4 phosphate-buffered saline (PBS) was irradiated with the 808 nm laser for 30 min with the power density at 0.8 W cm^2. The temperature was monitored by an IR thermal camera (Infrared Camera Inc.). The released DOX was removed by centrifugation. UV–vis–NIR spectra of Au–PEG + LA/DOX before and after laser irradiation were measured to determine the amount of released DOX. The Au–PEG + LA/DOX solution in pH 7.4 PBS without the laser irradiation was used as the control.

Cell culture experiment

Murine breast cancer cells (4T1) were cultured at 37°C under 5% CO_2. All cell culture related reagents were purchased from Invitrogen. 4T1 cells were cultured in standard RPMI-1640 medium containing 10% FBS and 1% penicillin/streptomycin. Cells were seeded into 96-well plates at a density of 1×10^4 cells per well and incubated with different concentrations of Au–PEG + LA/DOX or Au–PEG for 24 h. Relative cell viabilities were determined by the MTT assay.

In vitro combined therapy

For combination therapy, 4T1 cells were treated with Au–PEG + LA/DOX + laser, Au–PEG + LA/DOX, Au–PEG + LA + laser, DOX + laser and free DOX (DOX = 25 μM), and immediately irradiated by a 808 nm NIR laser at the power densities of 0.4 W/cm^2 and 0.8 W/cm^2 for 20 min, then washed with fresh cell medium and cultured for 24 h. The relative cell viabilities were then measured by the MTT assay. In order to investigate the cell uptake under the laser irradiation, all the cells under the same above treatment were incubated for 2 h, then were washed with PBS before confocal imaging (LeciaSP5 laser scanning confocal microscope).

Characterization

The morphology and structure of the product were characterized using a scanning electron microscope (SEM, JEOL, JSM-7000F) and a transmission electron microscope (TEM, JEOL, JEM-2100 with an accelerating voltage of 200 kV). The high-magnification TEM images of the product were obtained by scanning transmission electron microscopy (STEM, JEOL, JEM-ARM 200F). UV–vis–NIR spectra were taken by the Per-kin Elmer Lambda 750 UV–vis–NIR spectrophotometer. The IR laser for photothermal experiments is an 808 nm high power laser diode (Hi-Tech Optoelectronic Co. Ltd, Beijing, China). Confocal fluorescence images were taken by LeciaSP5 laser scanning confocal microscope.

Results

Materials fabrication & characterization

The 3D ordered mesoporous Au networks (Au networks in short) used in this study were prepared via a general soft-enveloping solid–liquid solution (SLS) phase interface reaction in KIT-6 hard template. Using hexane as the barrier layer and 1,1,3,3-tetramethyldisiloxane (TMDS) as the reduction agent to effectively prevent metal species from migrating to the outside of mesoporous channel, we successfully obtained Au networks (details in synthesis of 3D ordered mesoporous Au networks) [29]. Figure 2A and B showed the SEM and TEM images of typical Au networks after the removal of the silica template. The Au networks displayed monodispersed ordered porous structure and favorable homogeneity with average diameter of around 100 nm (Figure 2A) and the large-sized mesopores around 14–15 nm (Figure 2C). Figure 2D revealed the SAED pattern recorded from the white-boxed region in Figure 2B. The average diameter of Au networks exhibited a wide tunable capability by changing the reduction time. As shown in Supplementary Figure 1, the size of Au networks was regulated from 50 to 200 nm with the growth time from 10 min to 24 h. Owing to the novel 3D framework structure, characterized by high specific surface area, high internal porosity, and rough surface, Au networks would demonstrate diverse outstanding properties. In this work, we evaluated the Au networks as a multifunctional drug carrier for combination therapy of cancer.

Preparation of drug delivery system

As illustrated in Figure 1A, after removal the template, the Au networks were applied in photothermally enhanced chemotherapy of cancer. A convenient and effective strategy, which utilized one of the representative cancer chemotherapy agents [31,32], was adopted to load DOX into the mesoporous Au networks. In particular, the Au networks were first modified with PEG, and then the phase-change material LA (melting point, 43°C) was mixed well with DOX. After that, Au–PEG was mixed with LA/DOX, and the structure of Au–PEG + LA/DOX conjugate networks was well defined. As long as the drug was miscible with the LA phase, it could be conveniently transferred into the hollow interiors of networks. The LA would begin to melt when the temperature of Au networks raised beyond the melting point of it, and then the drug was released from the melted LA by diffusion (Figure 1B). Thus, this phase-change material seemed to be 'gatekeeper' to help load the drug and control the release of drug with temperature increasing.

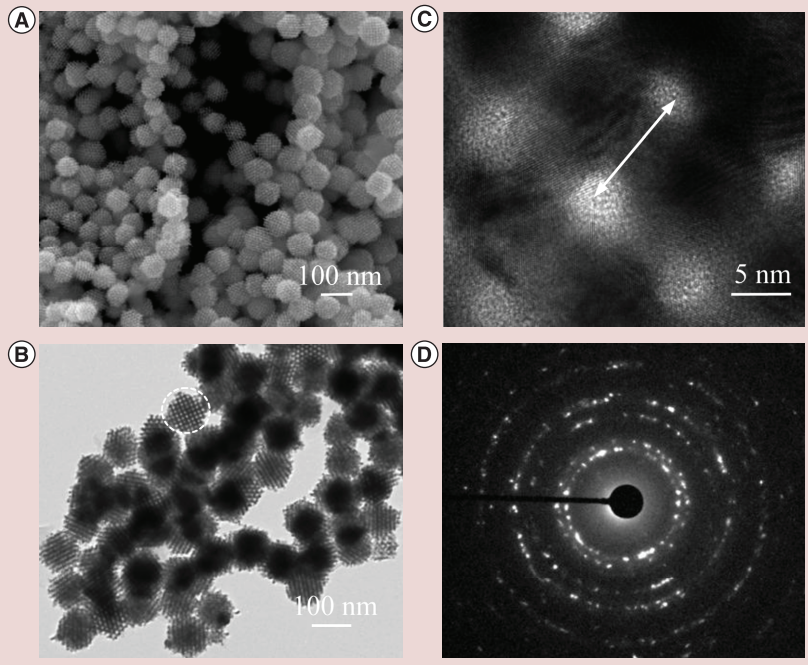

Figure 2. The typical morphology, structure and composition of Au networks. (A & B) The typical scanning electron microscopy and transmission electron microscopy images of Au networked structures. **(C)** The high-resolution transmission electron microscopy image of Au networks. The white arrow shows the size of one period at around 14–15 nm. **(D)** The selected area (electron) diffraction pattern recorded from the white-boxed region in Figure 2B.

For drug nanocarriers, the stability and size are important properties that influence their *in vivo* performance. These two factors will affect the biodistribution and circulation time of the carriers directly [33]. Stable and smaller particle sizes (<200 nm) can reduce the uptake of the reticulo endothelial system and provide efficient passive tumor-targeting ability via the enhanced permeability and retention effects [34]. Modified by PEG and loaded by LA/DOX, the final system of Au–PEG + LA/DOX could confine drug straightly, and exhibited excellent stability in physiological solutions (Figure 1C), providing the possibility for the *in vivo* application. Supplementary Figure 2 showed the dynamic light scattering size distribution of Au–PEG and Au–PEG + LA/DOX networks. After modified with PEG, the size of Au–PEG networks was around 150 nm and that of Au–PEG + LA/DOX networks around 165 nm. The increased size of micelles formed from Au–PEG might be due to the presence of DOX thick in the interior of LA.

Discussion

Photothermal effect

Thanks to the high NIR absorbance of Au networks [35,36], the obtained Au–PEG showed strong photothermal conversion efficiency and could be effectively heated up under exposure to an 808 nm NIR laser irradiation. We measured the photothermal effect of Au–PEG + LA/DOX networks in different concentrations as well as DI water. Figure 3A demonstrated, pure DI water did not show any significant response to the 808 nm irradiation at 1.0 W/cm^2, while the temperature of the Au–PEG + LA/DOX networks with the concentration of 0.1 mg/ml increased with the extension of irradiation time, reaching 43°C (the melting point of LA) in 2.5 min. This revealed excellent photothermal conversion characteristics at a shorter time, providing the possibility for clinical application. Besides, it could be easily seen that the heating rate and the final temperature were increased with the particle concentration. Under the same irradiation conditions, the temperatures of solution at 0.1, 0.2, 0.4 and 1.0 mg/ml can reach to 47.2, 52, 59 and 63°C in 5 min, respectively. Moreover, the photothermal conversion efficiency of Au networks has good advantages in comparison with many other PTT agents under the same condition, like carbon–silica inorganic nano-capsule with gold nanoparticle (Au@CSN) [27], monodisperse mesoporous Fe_3O_4 nanoparticles [25].

10.2217/nnm-2018-0242

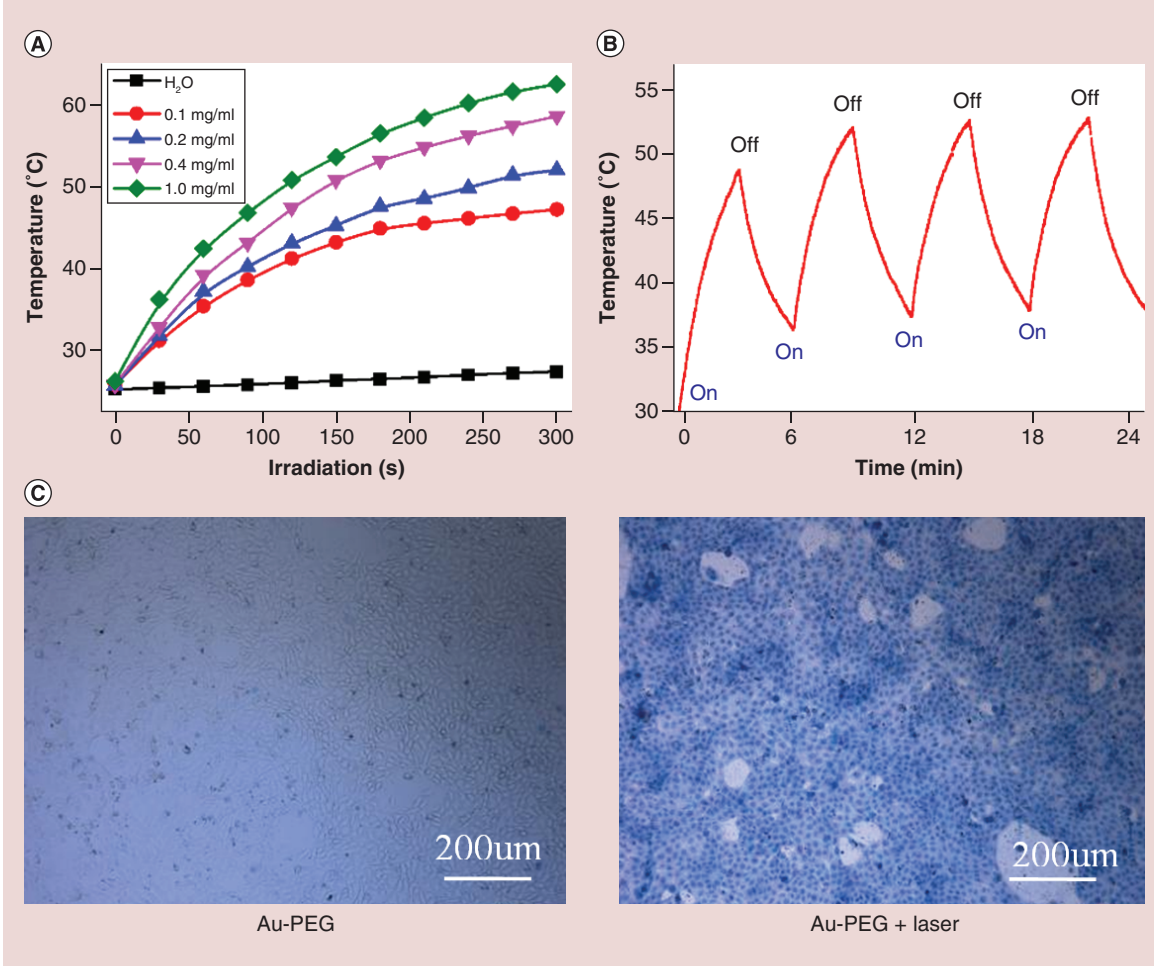

Figure 3. Biomedical application of Au networks and photothermal effect. (A) Photothermal heating curves of pure water and Au–PEG + LA/DOX solution with different concentrations (0.1, 0.2, 0.4 and 1.0 mg/ml) under 808 nm laser irradiation at the power density of 1 W/cm^2 for 5 min. **(B)** Temperature variations of Au–PEG + LA/DOX (0.1 mg/ml) under irradiation by 808 nm laser at the power density of 1 W/cm^2 for four cycles (6 min irradiation for each cycle). **(C)** Microscopic images of Trypan blue stained 4T1 cells with and without Au–PEG networks after being exposed to the 808 nm laser with the power density of 1 W/cm^2 for 5 min.

Furthermore, four cycles in every irradiation of 6 min by laser on/off were tested as shown in Figure 3B. The temperature of Au–PEG + LA/DOX networks was above 45°C at any cycle of laser, even at 0.1 mg/ml no significant tendency of the temperature decrease was observed until 24 min. Such photothermal system based on Au networks showed excellent photothermal stability after NIR laser radiation for multiple cycles. Importantly, the increase or decrease of temperature was consistent with laser presence or absence, illustrating that the change of temperature was simply controlled by the laser irradiation. This excellent photostability further allowed the synthesized Au networks to absorb light and convert it into heat during the laser irradiation.

Then, we used the Au–PEG networks as the photothermal agent for *in vitro* cancer cell ablation under laser irradiation (Figure 3C). The 4T1 cells were incubated in Au–PEG networks (0.1 mg/ml) for 24 h and then were exposed under 808 nm laser at 1 W/cm^2 for 5 min. After NIR laser exposure, dead cells were stained blue by treatment with Trypan blue. The microscope images showed no change for the control groups (without laser). At the same time, the majority of cells were destroyed after being incubated with 0.1 mg/ml of Au–PEG networks. The concentration of the photothermal agent (0.1 mg/ml), irradiation time (5 min), especially the lower laser power density (1 W/cm^2) are much lower than many previous reported *in vitro* cell ablation experiments using other photothermal agents, such as Au nanoflowers [37], Au–Pd bimetallic nanoflowers [38] and Au@carbon/calcium

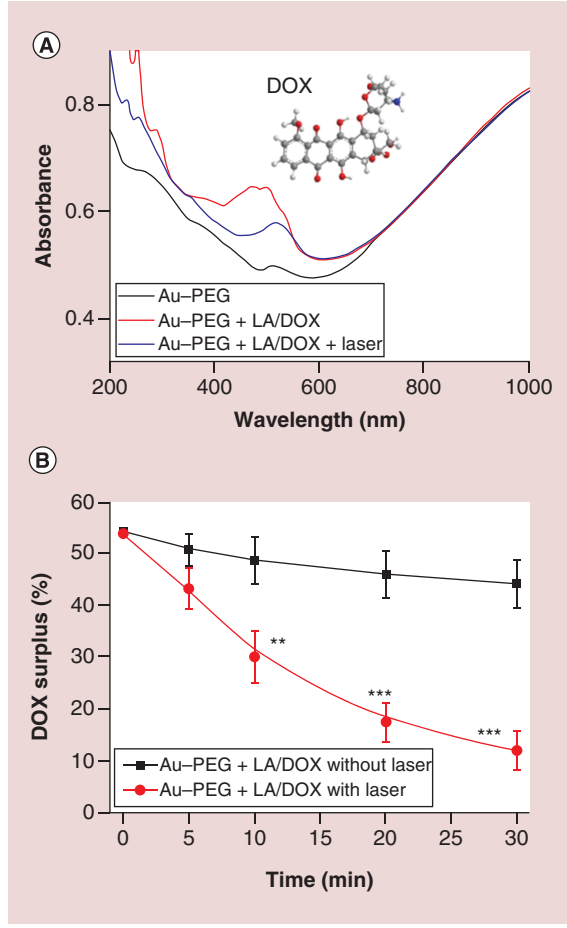

Figure 4. Drug controlled release. (A) Ultraviolet–visible–near-infrared reflectance spectra of Au–PEG, Au–PEG + LA/DOX, and Au–PEG + LA/DOX after 808 nm laser irradiation for 10 min. **(B)** DOX surplus of the Au–PEG + LA/DOX with or without 808 nm laser irradiation for different periods of time (1 W/cm^2). Statistical analysis was performed using the student's two-tailed t test: **$p < 0.01$; ***$p < 0.001$.
DOX: Doxorubicin; LA: Lauric acid; NIR: Near-infrared reflectance; PEG: Polyethene glycol.

phosphate nanoparticles [39]. The result further proved that under the laser irradiation, the Au–PEG networks would heat up through photothermal effect to kill the cancer cell.

Drug loading & release

Next, UV–vis–NIR spectra were used to check the loading efficiency of 3D mesoporous Au networks. Figure 4A showed absorption spectra of aqueous Au–PEG, Au–PEG + LA/DOX and Au–PEG + LA/DOX networks under laser irradiation. It was worth pointing out that the Au–PEG networks loaded with LA/DOX mixture also exhibited the characteristic absorption peak of the DOX at 480 nm, confirming successful encapsulation of the DOX inside the Au–PEG networks. The highest drug loading ratio was determined to be 54.2%, which was much higher than of many conventional Au or nonmetal nanoparticle-based drug delivery systems, for example, gold nanoparticles (17% for DOX) [33], angiopep-2 decorated gold nanoparticles (9.7% for DOX) [40], the mesoporous Fe_3O_4 NPs (22.6% for DOX) [25], protein-gold clusters-capped mesoporous silica nanoparticles silica nanoparticles (32% for DOX, 40% for gemcitabin) [28]. This distinction was attributed to the hollow internal structure and rough surface of the Au networks, which guaranteed the Au–PEG + LA/DOX system as a new kind of high-efficiency drug carrier.

The UV–vis–NIR spectra were also used to check the drug release of Au networks. As shown in Figure 4A, the characteristic peak of the DOX in Au–PEG + LA/DOX networks almost disappeared after laser irradiation, that is, under laser irradiation the drug diffused from Au–PEG + LA/DOX networks in virtue of the temperature increase. Moreover, the drug release behavior of Au–PEG + LA/DOX networks was investigated under 808 nm laser irradiation condition (Figure 4B). Here, only 10.16% of the DOX was released from Au–PEG + LA/DOX networks (initial DOX loading ratio: 52.4%) without laser irradiation in 30 min, implying that it was feasible for this system with phase-change material to be used as the carrier for controlled drug release due to the lower release rate (without laser irradiation). Compared with the sample without laser irradiation, 41.85% of loading drug was

10.2217/nnm-2018-0242

released from the Au–PEG + LA/DOX networks within half an hour under laser irradiation. The release rate of DOX under laser irradiation was much higher than that without laser irradiation. The underlying mechanism might be that the laser caused the temperature of the drug system of Au–PEG + LA/DOX increased above the melting point of LA, leading to drug release; on the other hand, once the laser was switched off, the system temperature dropped down below the melting point of LA, resulting in LA changed from liquid phase to solid phase to end up the drug release [26]. Moreover, due to the absorption in NIR, the temperature of this system with Au networks could be simply regulated by adjusting the duration of exposure rather than a more complex pH-controlled system [23,41] that needs extra handing and lower pH, accordingly providing a valid approach for drug release-accurate control of cancer drugs release with the temperature increasing of photothermal conversion.

The *in vitro* behavior of the controlled release-system based on Au–PEG + LA/DOX networks was then studied. The potential toxicity of this system on 4T1 murine breast cancer cells was first tested, and the standard MTT was used to determine the relative viabilities of the sample [42,43]. After incubation with different concentrations of Au–PEG for 24 h, no obvious toxicity of the cells was found at concentration of 100 μg/ml (Supplementary Figure 3), and the relative cell viability in every sample was close to 100%, presenting the good biocompatibility of this system, which is very important for cancer drugs to be used in living cells [44]. Loading with LA/DOX, the Au–PEG + LA/DOX networks were able to kill cancer cells by a concentration-dependent manner similar to the free DOX, shown in Supplementary Figure 4. After incubation for 24 h, the relative cell viability of Au–PEG + LA/DOX was below 20% with 50 μM of DOX, as well as the free DOX. At the same time, the toxicity of Au–PEG + LA/DOX networks with different concentration of DOX was below but close to free DOX, making it possible to apply in cancer treatment.

Combination treatment of photothermal therapy & chemotherapy

The combination of photothermal with chemotherapy delivered by the system of Au–PEG + LA/DOX networks was then studied. According to recent study, mild hyperthermia can also increase cell permeability and further promote the effect of cancer therapy [45–48]. To test whether the heat generated by Au–PEG networks and Au–PEG + LA/DOX networks could be utilized to promote the efficiency of chemotherapy. Au–PEG, Au–PEG + LA/DOX and free DOX (DOX = 25 μM) were cultured with 4T1 cells for 20 min with or without 808 nm laser irradiation at a power density of 0.4 and 0.8 W/cm^2, which could generate moderate heat and raise the temperature of the medium to around 43°C, and then Au–PEG, Au–PEG + LA/DOX, and DOX were washed with fresh cell medium and cultured for 24 h. As it shown in Figure 5A, the cell viability of DOX with or without laser was little difference, showing the effect of laser was almost negligible for free DOX. At the same time, with increasing the power density from 0.4 to 0.8 W/cm^2, the cell viability of Au–PEG + LA decreased from 86.9 to 70.7% in 20 min, indicating that the photothermal conversion of Au–PEG + LA was increased with the power density in short time. Moreover, the drug was released as temperature rise, which motivated the combination of photothermal with chemotherapy. Extraordinarily, according to the operation data, the Au–PEG + LA/DOX networks showed a great improvement of anticancer effect when heightening the power density, and the cell viability from 44.2% at 0.4 W/cm^2 fell to 13.2% at 0.8 W/cm^2, while the cell viability of the control group did not decrease significantly. The Au–PEG + LA/DOX networks at lower power density (under 1.0 W/cm^2) within 20 min used in our experiment showed almost the same effect for chemo-photothermal cancer therapy instead of several hours in most reported nanostructures [27,49]. This demonstrated that the Au networks showed a much better performance with the present of DOX for photothermally enhanced chemotherapy of cancer.

In order to investigate the cell uptake under the laser irradiation, all the cells under the same above treatment were incubated for 2 h, then were washed with PBS before confocal imaging. Once the drug was released, the DOX molecules in the cytosol would be rapidly transported to the nucleus and avidly bound to the chromosomal DNA [50]. From the confocal fluorescence imaging (Figure 5B & C), the remarkably enhanced DOX fluorescence was observed in the cells incubated with Au–PEG + LA/DOX post laser exposure compared with no laser irradiation, suggesting the high cell uptake of DOX from the nano-carriers facilitated by a LA-receptor-mediated. Interestingly, obvious DOX fluorescence was noted inside cell nuclei than the cytoplasm for Au–PEG + LA/DOX networks incubated cells after laser irradiation as a result of drug release, but not for those without light exposure. These results clearly indicated that the Au–PEG + LA/DOX networks were transported into cells through a nonspecific endocytosis mechanism and the drug release were greatly controlled through laser irradiation.

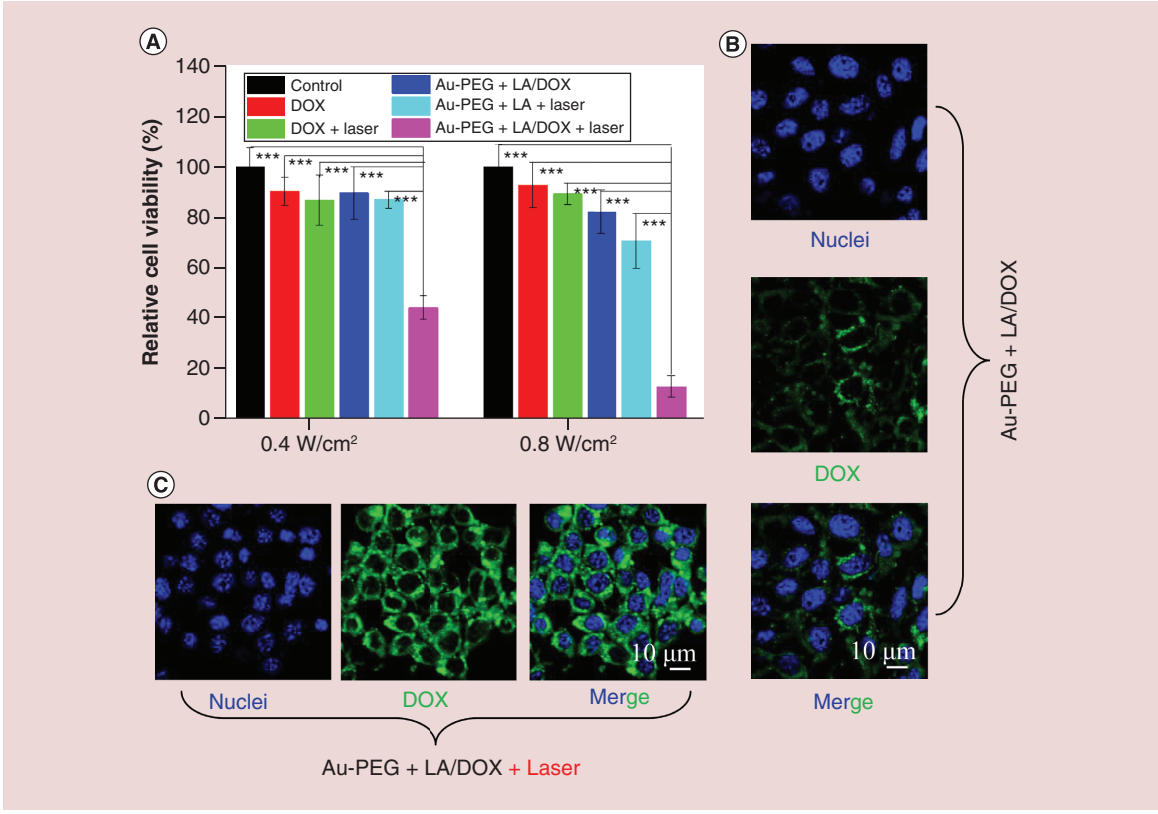

Figure 5. The combination of photothermal with chemotherapy. (A) Relative viabilities of 4T1 cells after various treatments. In this experiment, 4T1 cells were incubated with Au–PEG + LA/DOX + laser, Au–PEG + LA/DOX, Au–PEG + LA + laser, DOX + laser, and free DOX (DOX = 25 μM), and immediately irradiated by a 808 nm near-infrared reflectance laser at the power densities of 0.4 and 0.8 W/cm^2 for 20 min, then washed with fresh cell medium and cultured for 24 h before the MTT assay. **(B)** Confocal fluorescence images of 4T1 cells incubated with Au–PEG + LA/DOX, (DOX = 25 μM) and **(C)** immediately irradiated by a 808 nm NIR laser at the power density 0.8 W/cm^2 for 20 min, then washed with fresh cell medium and cultured for 2 h.
Statistical analysis was performed using the student's two-tailed t-test: ***$p < 0.001$.
DOX: Doxorubicin; LA: Lauric acid; PEG: Polyethene glycol.

Therefore, it can be concluded that NIR-light triggered intracellular drug release of Au–PEG + LA/DOX networks system in such combined photothermal and chemotherapy could offer an apparent synergistic effect to destruct cancer cells [51].

Conclusion

In this work, we reported a new class of multifunctional drug delivery based on the 3D mesoporous structured Au networks to apply in photothermally enhance chemotherapy of cancer. The Au networks were decorated by PEG and filled with LA/DOX, exhibiting excellent photothermal conversion efficiency with high drug loading efficiency (DOX, 54.2%). Under 808 nm laser irradiation, the temperature of the Au–PEG + LA/DOX networks system could raise to around 45°C (above the melting point of LA) in 2.5 min, leading to controlled drug release. Thus, the novel system of Au–PEG + LA/DOX networks shows outstanding biological performance in controllable drug delivery capability and combination of photothermal and chemotherapy [52,53], offering references for cancer therapy.

Future perspective

Cancer therapy holds great potential because of the high mortality rate all the time. Though many methods were presented, the drug delivery was still a hardship in cancer therapy due to the lower drug loading ratio and difficulty to realize ideal control of drug release in a simple way. The authors of this manuscript reported a biocompatible and temperature responsive controlled drug delivery system based on 3D mesoporous structured Au networks, which

10.2217/nnm-2018-0242

represents a new class of drug-loading agents. Modified with PEG, mixed with LA/DOX and the final system showed a high drug loading and could release the drug with the temperature increase.

The cancer treatment will be improved in the future by the use of nanomaterial with advanced properties. Further study would pay more attention on drug release and combining with the photothermal and chemotherapy.

Summary points

- A well-defined biocompatible and temperature responsive controlled drug delivery system was synthesized with tunable size, near-infrared reflectance absorbance and mesoporous structured Au networks.
- Excellent photothermal conversion efficiency and high drug loading were achieved by the drug synthesis with the help of the phase-change material.
- The drug delivery system may play an important role in controllable drug delivery capability and combination of photothermal and chemotherapy.

Supplementary data

To view the supplementary data that accompany this paper please visit the journal website at: www.futuremedicine.com/doi/full/10.2217/nnm-2018-0242

Author contributions

L Zhang synthesized the materials and carried out the characterizations of the structures. L Lu, C Ma and Y Dai completed the TEM, EDX Mapping and HR-TEM characterizations. S Shen, L Zhang and L Cheng conducted the biology performance measurements. L Zhang, L Cheng and J Fang designed, supervised the project and wrote the manuscript. All authors discussed the results and commented on the manuscript.

Financial & competing interests disclosure

This work was supported by the National Natural Science Foundation of China (grant numbers: 21675122, 51171139 and 21874104), the Key Research Program in Shaanxi (grant number 2017NY-114), the World-Class Universities (Disciplines) and the Characteristic Development Guidance Funds for the Central Universities. The authors have no other relevant affiliations or financial involvement with any organization or entity with a financial interest in or financial conflict with the subject matter or materials discussed in the manuscript apart from those disclosed.

No writing assistance was utilized in the production of this manuscript.

References

Papers of special note have been highlighted as: • of interest; •• of considerable interest

1. Ayalaorozco C, Urban C, Knight MW *et al.* Au nanomatryoshkas as efficient near-infrared photothermal transducers for cancer treatment: benchmarking against nanoshells. *ACS Nano* 8(6), 6372–6381 (2014).
2. Wicki A, Witzigmann D, Balasubramanian V, Huwyler J. Nanomedicine in cancer therapy: challenges, opportunities, and clinical applications. *J. Control. Rel.* 200, 138–157 (2015).
3. Kong FY, Zhang JW, Li RF, Wang ZX, Wang WJ, Wang W. Unique roles of gold nanoparticles in drug delivery, targeting and imaging applications. *Molecules* 22(9), pii: E1445 (2017).
4. Hardiansyah A, Huang LY, Yang MC *et al.* Magnetic liposomes for colorectal cancer cells therapy by high-frequency magnetic field treatment. *Nanoscale Res. Lett.* 9(1), 497 (2014).
5. Bulbake U, Doppalapudi S, Kommineni N, Khan W. Liposomal formulations in clinical use: an updated review. *Pharmaceutics* 9(2), 12 (2017).
6. Meng F, Hennink WE, Zhong Z. Reduction-sensitive polymers and bioconjugates for biomedical applications. *Biomaterials* 30(12), 2180–2198 (2009).
7. Zare-Zardini H, Taheri-Kafrani A, Amiri A, Bordbar AK. New generation of drug delivery systems based on ginsenoside rh2-, lysine- and arginine-treated highly porous graphene for improving anticancer activity. *Sci. Rep.* 8(1), 586 (2018).
8. Chen Y. Two-dimensional graphene analogues for biomedical applications. *Cheminform* 44(9), 2681–2701 (2015).
9. Boncel S, Zając P, Koziol KKK. Liberation of drugs from multi-wall carbon nanotube carriers. *J. Control. Rel.* 169(1–2), 126–140 (2013).
10. Luo Z, Cai K, Hu Y *et al.* Redox-responsive molecular nanoreservoirs for controlled intracellular anticancer drug delivery based on magnetic nanoparticles. *Adv. Mater.* 24(3), 431–435 (2012).

• **Obtains a novel redox-responsive controlled drug release system based on magnetic nanoparticles.**

11. Hu Y, Cai K, Luo Z, Jandt KD. Layer-by-layer assembly of β-estradiol loaded mesoporous silica nanoparticles on titanium substrates and its implication for bone homeostasis. *Adv. Mater.* 22(37), 4146–4150 (2010).
12. Croissant JG, Fatieiev Y, Almalik A, Khashab NM. Mesoporous silica and organosilica nanoparticles: physical chemistry, biosafety, delivery strategies, and biomedical applications. *Adv. Healthcare Mater.* 7(4) (2018).10.1002/adhm.201700831
13. Song J, Zhou J, Duan H. Self-assembled plasmonic vesicles of SERS-encoded amphiphilic gold nanoparticles for cancer cell targeting and traceable intracellular drug delivery. *J. Am. Chem. Soc.* 134(32), 13458–13469 (2012).
14. Jain PK, El-Sayed IH, El-Sayed MA. Au nanoparticles target cancer. *Nano Today* 2(1), 18–29 (2007).
15. Liu Z, Cheng L, Zhang L, Yang Z, Liu Z, Fang J. Sub-100nm hollow Au–Ag alloy urchin-shaped nanostructure with ultrahigh density of nanotips for photothermal cancer therapy. *Biomaterials* 35(13), 4099–4107 (2014).

• **Employs the hollow Au-Ag alloy nanourchins (HAAA-NUs) with sub-100 nm in size for applications in photothermal cancer treatment.**

16. Cui H, Hu D, Zhang J *et al.* Gold nanoclusters-indocyanine green nanoprobes for synchronous cancer imaging, treatment, and real-time monitoring based on fluorescence resonance energy transfer. *ACS Appl. Mater. Interfaces* 9(30), 25114–25127 (2017).
17. An L, Wang Y, Tian Q, Yang S. Small gold nanorods: recent advances in synthesis, biological imaging, and cancer therapy. *Materials* 10(12), 1372 (2017).
18. Sengani M, Grumezescu AM, Rajeswari VD. Recent trends and methodologies in gold nanoparticle synthesis – a prospective review on drug delivery aspect. *OpenNano* 2, 37–46 (2017).
19. Khalil I, Julkapli NM, Yehye WA, Basirun WJ, Bhargava SK. Graphene–gold nanoparticles hybrid-synthesis, functionalization, and application in a electrochemical and surface-enhanced raman scattering biosensor. *Materials* 9(6), 406 (2016).
20. Liu J, Yang G, Zhu W *et al.* Light-controlled drug release from singlet-oxygen sensitive nanoscale coordination polymers enabling cancer combination therapy. *Biomaterials* 146(39), 40–48 (2017).
21. Saber MM, Bahrainian S, Dinarvand R, Atyabi F. Targeted drug delivery of Sunitinib Malate to tumor blood vessels by cRGD–chiotosan–gold nanoparticles. *Int. J. Pharm.* 517(1-2), 269–278 (2016).
22. Wang F, Wang YC, Dou S, Xiong MH, Sun TM, Wang J. Doxorubicin-tethered responsive gold nanoparticles facilitate intracellular drug delivery for overcoming multidrug resistance in cancer cells. *ACS Nano* 5(5), 3679–3692 (2011).
23. Faheem M, Mingyi G, Wenxiu Q *et al.* pH-triggered controlled drug release from mesoporous silica nanoparticles via intracelluar dissolution of ZnO nanolids. *J. Am. Chem. Soc.* 133(23), 8778–8781 (2011).
24. Wang J, Yang P, Cao M *et al.* A novel graphene nanodots inlaid porous gold electrode for electrochemically controlled drug release. *Talanta* 147, 184–192 (2016).
25. Zhang QI, Liu J, Yuan K, Zhang Z, Zhang X, Fang X. A multi-controlled drug delivery system based on magnetic mesoporous Fe_3O_4 nanopaticles and a phase change material for cancer thermo-chemotherapy. *Nanotechnology* 28(40), 405101 (2017).
26. Moon GD, Choi SW, Cai X *et al.* A new theranostic system based on gold nanocages and phase-change materials with unique features for photoacoustic imaging and controlled release. *J. Am. Chem. Soc.* 133(13), 4762–4765 (2011).

•• **Presents a facile and versatile strategy for loading either hydrophobic or hydrophilic drugs into the hollow interiors of Au nanocages.**

27. Li L, Chen C, Liu H *et al.* Multifunctional carbon–silica nanocapsules with gold core for synergistic photothermal and chemo-cancer therapy under the guidance of bimodal imaging. *Adv. Funct. Mater.* 26(24), 4252–4261 (2016).
28. Croissant JG, Zhang D, Alsaiari S *et al.* Protein–gold clusters-capped mesoporous silica nanoparticles for high drug loading, autonomous gemcitabine/doxorubicin co-delivery, and *in-vivo* tumor imaging. *J. Control. Rel.* 229, 183–191 (2016).
29. Fang J, Zhang L, Li J *et al.* A general soft-enveloping strategy in the templating synthesis of mesoporous metal nanostructures. *Nat. Commun.* 9(1), 521 (2018).
30. Cheng L, Yang K, Li Y *et al.* Facile preparation of multifunctional upconversion nanoprobes for multimodal imaging and dual-targeted photothermal therapy. *Angew. Chem. Int. Edit.* 50(32), 7385–7390 (2011).
31. Mussi SV, Sawant R, Perche F *et al.* Novel nanostructured lipid carrier co-loaded with doxorubicin and docosahexaenoic acid demonstrates enhanced *in vitro* activity and overcomes drug resistance in MCF-7/Adr cells. *Pharm. Res.* 31(8), 1882–1892 (2014).
32. Liu Y, Fang J, Kim YJ, Wong MK, Wang P. Codelivery of doxorubicin and paclitaxel by cross-linked multilamellar liposome enables synergistic antitumor activity. *Mol. Pharm.* 11(5), 1651–1661 (2014).
33. Prabaharan Mani, Grailer JJ *et al.* Gold nanoparticles with a monolayer of doxorubicin-conjugated amphiphilic block copolymer for tumor-targeted drug delivery. *Biomaterials* 30(30), 6065–6075 (2009).
34. Schmalenberg KE, Frauchiger L, Nikkhouyalbers L, Uhrich KE. Cytotoxicity of a unimolecular polymeric micelle and its degradation products. *Biomacromolecules* 2(3), 851–855 (2001).
35. Huang X, El-Sayed IH, Qian W, El-Sayed MA. Cancer cell imaging and photothermal therapy in the near-infrared region by using gold nanorods. *J. Am. Chem. Soc.* 128(6), 2115–2120 (2006).

36. Ye X, Shi H, He X, Wang K, Li D, Qiu P. Gold nanorod-seeded synthesis of Au@Ag/Au nanospheres with broad and intense near-infrared absorption for photothermal cancer therapy. *J. Mater. Chem. B* 2(23), 3667–3673 (2014).
37. Li S, Zhang L, Wang T, Li L, Wang C, Su Z. The facile synthesis of hollow Au nanoflowers for synergistic chemo-photothermal cancer therapy. *Chem. Commun.* 51(76), 14338–14341 (2015).
38. Qian L, Yang X. Polyamidoamine dendrimers-assisted electrodeposition of gold−platinum bimetallic nanoflowers. *J. Phys. Chem. B* 110(33), 16672–16678 (2006).
39. Wang H, Zhang M, Zhang L *et al.* Near-infrared light and pH-responsive Au@carbon/calcium phosphate nanoparticles for imaging and chemo-photothermal cancer therapy of cancer cells. *Dalton T.* 46(43), 14746–14751 (2017).
40. Ruan S, Yuan M, Zhang L *et al.* Tumor microenvironment sensitive doxorubicin delivery and release to glioma using angiopep-2 decorated gold nanoparticles. *Biomaterials* 37, 425–435 (2015).
41. Iyisan B, Kluge J, Formanek P, Voit B, Appelhans D. Multifunctional and dual-responsive polymersomes as robust nanocontainers: design, formation by sequential post-conjugations, and pH-controlled drug release. *Chem. Mater.* 28(5), 1513–1525 (2016).
42. Zhao Y, Peng J, Li J *et al.* Tumor-targeted and clearable human protein-based MRI nanoprobes. *Nano Lett.* 17(7), 4096–4100 (2017).
43. Chen LY, Wang CW, Yuan Z, Chang HT. Fluorescent gold nanoclusters: recent advances in sensing and imaging. *Anal. Chem.* 87(1), 216–229 (2015).
44. Nahire R, Haldar MK, Paul S *et al.* Multifunctional polymersomes for cytosolic delivery of gemcitabine and doxorubicin to cancer cells. *Biomaterials* 35(24), 6482–6497 (2014).
45. Tian B, Wang C, Zhang S, Feng L, Liu Z. Photothermally enhanced photodynamic therapy delivered by nano-graphene oxide. *ACS Nano* 5(9), 7000–7009 (2011).
46. Yuan J, Liu J, Song Q *et al.* Photoinduced mild hyperthermia and synergistic chemotherapy by one-pot-synthesized docetaxel-loaded poly(lactic-co-glycolic acid)/polypyrrole nanocomposites. *ACS Appl. Mater. Interfaces* 8(37), 24445–24454 (2016).
47. Alahmady ZS, Aljamal WT, Bossche JV *et al.* Lipid-peptide vesicle nanoscale hybrids for triggered drug release by mild hyperthermia *in vitro* and *in vivo*. *ACS Nano* 6(10), 9335–9346 (2012).
48. Jung BK, Lee YK, Hong J, Ghandehari H, Yun CO. Mild hyperthermia induced by gold nanorod-mediated plasmonic photothermal therapy enhances transduction and replication of oncolytic adenoviral gene delivery. *ACS Nano* 10(11), 10533–10543 (2016).
49. Yang Q, Peng J, Xiao Y *et al.* Porous Au@Pt nanoparticles: therapeutic platform for tumor chemo-photothermal co-therapy and alleviating doxorubicin-induced oxidative damage. *ACS Appl. Mater. Interfaces* 10(1), 150–164 (2017).
50. Gabbay EJ, Grier D, Fingerle RE *et al.* Interaction specificity of the anthracyclines with deoxyribonucleic acid. *Biochemistry* 15(10), 2062 (1976).
51. Gillies ER, Fréchet JM. pH-responsive copolymer assemblies for controlled release of doxorubicin. *Bioconjugate Chem.* 16(2), 361–368 (2005).
52. Zhu C, Du D, Eychmüller A, Lin Y. Engineering ordered and nonordered porous noble metal nanostructures: synthesis, assembly, and their applications in electrochemistry. *Chem. Rev.* 115(16), 8896–8943 (2015).
53. Li J, Hu Y, Hou Y *et al.* Phase-change material filled hollow magnetic nanoparticles for cancer therapy and dual modal bioimaging. *Nanoscale* 7(19), 9004–9012 (2015).

- **Demonstrates sensitive thermal response to alternating current magnetic field (AMF) for triggering switchable controlled drug delivery with 'zero release' feature.**